Photonic-band-edge-induced lasing in self-assembled dye-activated photonic crystals

Rajesh V. Nair,[1,*] Anjani K. Tiwari,[2] Sushil Mujumdar,[2] and B. N. Jagatap[1]

[1]*Atomic and Molecular Physics Division, Bhabha Atomic Research Centre, Mumbai, India 400 085*
[2]*Nano-Optics and Mesoscopic Optics Laboratory, Tata Institute of Fundamental Research, Mumbai, India 400 005*

We report experimental demonstration of photonic band-edge lasing in three-dimensionally ordered self-assembled photonic crystals consisting of rhodamine-B dye doped nanospheres of diameter 295 nm. Our all-solid photonic crystal shows a well-resolved photonic stop gap in the visible region. Laser-induced emission experiments reveal more than 51% inhibition in spontaneous emission intensity of dye molecules within the stop gap and an enhancement near the blue side of the stop gap. With increase in incident pump energy, we achieve photonic-band-edge-induced lasing at room temperature with a lasing threshold of 0.7 mJ. We explain the origin of lasing as due to the enhancement of local density of states near the band edges and the light field distribution within the photonic crystal structure. Our results indicate that such all-solid, dye-activated self-assembled nanostructures are a promising candidate for realizing photonic devices.

I. INTRODUCTION

Tailoring light emission using engineered nanophotonic structures is an active area of research due to its potential applications in single-photon generation [1], miniature lasers [2], light emitting diodes [3], and solar energy harvesting [4]. This can be achieved owing to the possibility of tuning the local density of states (LDOS) of photons and hence the spontaneous emission by engineering the nanophotonic structures [5]. Photonic-band-gap structures or photonic crystals belong to a class of nanophotonic structures where the dielectric constant is periodically altered along three orthogonal directions with a period of the order of the wavelength of light [6,7]. Because of the translational periodicity of the structure, the dispersion relation for photons is organized into a series of allowed or forbidden bands similar to semiconductors. Frequency ranges can appear in the dispersion diagram wherein light is not allowed to couple to the structure along particular directions of propagation, leading to photonic stop gaps. When the stop gap along different directions of propagation overlaps for different polarization states of the incident light, it results in a three-dimensional (3D) photonic band gap [8]. As a consequence of this, the allowed LDOS for those forbidden frequencies of light vanishes inside the photonic band gap and is enhanced near the band edges. Therefore, tailoring the LDOS via engineering the photonic-band-gap structures can control the emission properties in any frequency range and for different polarization states of light [5,9]. Such control of LDOS opens eminent opportunities in quantum electrodynamics and quantum information processing.

An important consequence of vanishing LDOS is the inhibition of spontaneous emission [9]. This inhibition of spontaneous emission in the photonic band gap can be exploited for achieving low-threshold lasing [6]. In this case the inversion is easier to achieve because the spontaneous emission is suppressed [10]. It is an extremely challenging task to achieve a photonic band gap due to harsh constraints such as the crystal symmetry and requisite refractive index

contrast in the constituent building blocks [8,11]. By removing the constraint of refractive index contrast, one can still achieve a photonic stop gap that exhibits light inhibition only in certain directions. This facilitates the understanding of light propagation in periodic structures and their potential applications using relatively simpler structures [12]. In this context, 3D-ordered self-assembled colloidal photonic crystals with stop gaps have received a lot of attention in recent years [13].

Spontaneous emission rates of light sources depend on the LDOS through the well-known Fermi golden rule [5]. Accordingly, the emission intensity and the rate decrease inside the photonic stop gap with the reduction of the LDOS. Inhibition of spontaneous emission of dyes and quantum dots has been observed in self-assembled colloidal photonic crystals [9,14–17]. The enhancement of LDOS in the frequency range of the stop gap can be achieved by creating intentional defects that effectively act as cavities with high quality factors in the otherwise periodic structure [2]. This enhancement in LDOS leads to an increased spontaneous emission rate when the cavity mode frequency is resonant with the emission frequency of the emitters [18]. This is another regime in nanophotonic structures to achieve low-threshold lasing through channeling the spontaneously emitted photons into the stimulated emission process. This is manifested through the β-parameter, defined as the number of spontaneously emitted photons contributing to the stimulated emission process per total number of spontaneously emitted photons. A sought-after goal in nanophotonics research is to reach $\beta = 1$, or the so-called thresholdless laser, wherein the light-in-light-out (L-L) curve shows a straight line behavior [19,20].

In a photonic crystal without cavities, an enhancement of LDOS can also occur at the photonic band-edge frequencies [21]. Near the band edges, the photonic bands become nearly flat, resulting in a reduced group velocity for light so that light-matter interaction is enhanced. The LDOS is inversely proportional to the group velocity and therefore it is enhanced at the edges. Various fundamental phenomena and applications in the realm of lasing and nonlinear optics are forecast at the band-edge frequencies [22,23]. Photonic-band-edge-induced

*rvnair@barc.gov.in

lasing in the near ultraviolet has been observed for ZnO inverse opal photonic crystals in the first- and second-order stop gaps and in liquid-crystal-based one-dimensional photonic crystal films [24–27]. Lasing is demonstrated along a particular direction by infiltrating conducting polymers and laser dye solutions in self-assembled colloidal photonic crystals [28–30]. Inverse opal photonic crystals infiltrated with dyes are also used for realizing lasing in the visible wavelength range [31]. In these studies, photonic crystal structures are first synthesized and then the gain medium (e.g., laser dye) is infiltrated. Such systems have some demerits. Inverse opal based photonic crystal structures involve complex fabrication processes and hence are susceptible to fabrication defects, apart from yielding very small sample sizes. Moreover, the fabrication processes for inverse opals tend to be protracted. In actual lasing experiments, they need to be immersed in dye-based liquids, which reduce the refractive index contrast apart from posing serious complications in practical applications. For these reasons, it is important to provide quick-to-fabricate, large-sized, functional alternatives to inverse opals in order to achieve lasing action from solid nanophotonic structures.

In this article, we present results on all-solid samples consisting of self-assembled colloidal photonic crystals made of dye-activated polymer nanospheres. We report room temperature lasing in the visible wavelength region occurring near the photonic band-edge frequencies. These large-area crystals can be prepared in a time span of three hours. In these photonic crystals, the gain medium is doped into each building block, which is a nanosphere in this work, thus avoiding post infiltration of the gain medium. This results in a uniform distribution of gain medium everywhere inside the photonic crystal with zero gain in the surroundings. In infiltrated samples, the surrounding infiltrant liquid can create optical gain that is not in the band-edge mode, compromising a clear band-edge lasing signal. We study the suppression of spontaneous emission at the photonic stop gap wavelengths, and an enhancement in emission over a broad range of wavelengths at the blue side of the stop gap. At higher excitation energy, we achieve lasing at the low-frequency photonic band edge with a lasing threshold of 0.7 mJ. We explain the origin of lasing as due to the enhanced LDOS at the band edges and the field intensity distribution within the photonic crystal structures. Our results have implications in the lasing process from different kind of photonic nanostructures. Since our photonic crystals are all solid, it is a promising candidate for future photonic applications.

This paper is organized as follows: The experimental procedure used for the photonic crystal synthesis and their characterization is briefly explained in Sec. II. Detailed analysis of laser-induced emission results are presented in Sec. III. Inhibition of spontaneous emission and the occurrence of band-edge lasing is detailed here. Important conclusions arising from this work are given in Sec. IV.

II. EXPERIMENTAL DETAILS

We use commercially available rhodamine-B-doped polystyrene (dyed-PS) colloidal suspensions of submicron diameters. The inward-growing self-assembling method is used for the synthesis of photonic crystals on a clean glass substrate [32]. We use 200 μL of 2.5 wt% colloids of diameter 295 nm for the synthesis of photonic crystals. Large area ($\sim$2 cm^2) photonic crystals are grown using this method in a time span of 3 hours. This diameter of nanospheres is specifically chosen so as to overlap the rhodamine-B dye emission, which is centered at 600 nm, with photonic stop gap along the [111] direction [14]. We also synthesized a reference sample using nanospheres of diameter 617 nm, doped with the same dye. The rhodamine-B dye emission does not overlap with the (111) photonic stop gap for this sphere diameter. Thus, the reference sample has the same photonic structure, the same packing fraction, and the same dye embedded, the only difference being in the stop-gap wavelength.

The structural quality of the photonic crystals is investigated using a field-emission scanning electron microscope (FESEM). The stop gap is measured from the reflectivity and transmittance spectra using a Perkin Elmer Lambda 950 spectrophotometer. The light source used is a halogen lamp with beam dimensions of 5 mm × 5 mm, the light beam being unpolarized. A silicon detector is used for collecting the reflected or transmitted light. Laser-induced-emission studies are performed using a frequency-doubled Nd:YAG laser as a pumping source at a wavelength of 532 nm and pulse duration of 6 ns. The light is focused on the sample using a lens of focal length 300 mm to an illumination spot of $\sim$1 mm. The emitted light is focused onto the input slit of a monochromator and detected with a charge coupled device (CCD).

III. RESULTS AND DISCUSSIONS

The structural quality of photonic crystals as seen in the FESEM is given in Figs. 1(a) and 1(b). The well ordering of spheres on the surface and in the depth of the photonic crystals is clearly evident. The hexagonal packing of spheres seen on the surface represents the (111) plane of the face
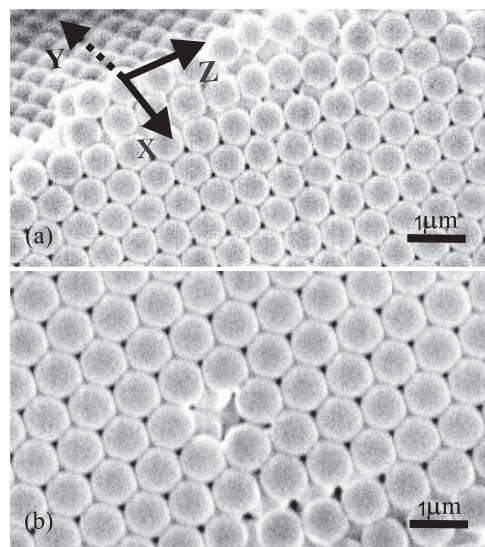

FIG. 1. (a) FESEM image of the photonic crystals made of dye doped PS spheres with a diameter of 295 nm indicates proper ordering of spheres on the surface and in the bulk of the crystal. (b) The top surface shown is representative of the (111) plane of the fcc lattice. Very good ordering of spheres is observed in (a) and (b).
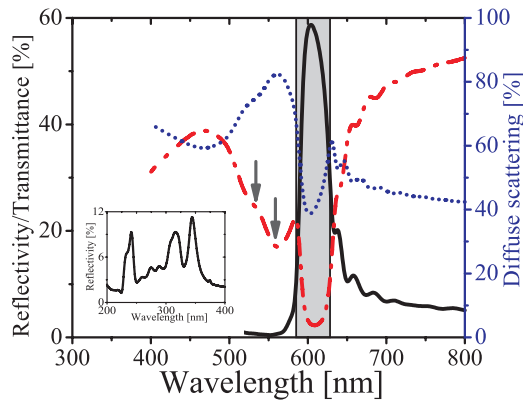
FIG. 2. (Color online) Reflectivity (black line), transmittance (red dash-dotted line), and diffuse scattered intensity (blue dotted line) measured from the (111) plane of the photonic crystal composed of dye doped PS sphere of diameter 295 nm. The peak in reflectivity spectra and trough in transmittance spectra are in good agreement, indicating the signature of a photonic stop gap. The absorption due to rhodamine-B dye is indicated using downward arrows in the transmittance spectra. The diffuse scattered intensity drops inside the stop gap but remains nonzero due to residual disorder present in the samples. The diffuse scattered intensity increases near the blue side of the stop gap. The inset shows the higher-order photonic stop gaps and their observation is a confirmation of superior optical quality of our samples.

centered cubic (fcc) lattice [32]. The optical studies discussed in the present work are measured from the (111) plane. The signature of a photonic stop gap is a peak in the reflectivity spectra, accompanied by a trough in the transmittance spectra. Figure 2 shows the reflectivity R (black line) and transmittance T (red dash-dotted line) measured from the (111) plane of the photonic crystals composed of dye doped PS spheres of diameter 295 nm. Reflectivity is measured at near-normal incidence ($\sim 8°$) and the transmittance is measured at normal incidence. The effect of crystal planes other than the (111) plane can be probed through angle-resolved reflectivity measurements [33]. The peak in reflectivity spectra with a reflectance of $\sim 59\%$ at a wavelength of 604 nm is accompanied by a trough in the transmission spectra with a transmittance of $\sim 2.4\%$, indicating the photonic stop gap.

The photonic strength or the full width at half maximum (FWHM) of the reflectivity peak is estimated to be 6.1%, which is close to the calculated values for similar photonic crystal structures [14,15]. The Bragg length L_B (i.e., the distance through which light propagates in the photonic stop gap) is estimated to be 2.5 μm. The Fabry-Pérot (FP) oscillations seen around the photonic stop gap is evidence of the uniform thickness of the sample, and the identical orientation of the crystal domains. The thickness (t) [34] estimated using FP fringes in the long-wavelength side away from the stop gap is 7 μm and hence $t \sim 2.8 L_B$. This size is comparable to the best reported sample in terms of thickness and is theoretically known to provide sufficient photonic strength [35]. The thickness ensures that the sample is immune to finite-size effects. In the wavelength range of 500 to 550 nm, the transmission spectra show an abrupt decrease, which is due to the absorption of the rhodamine-B dye (downward arrow in Fig. 2) and
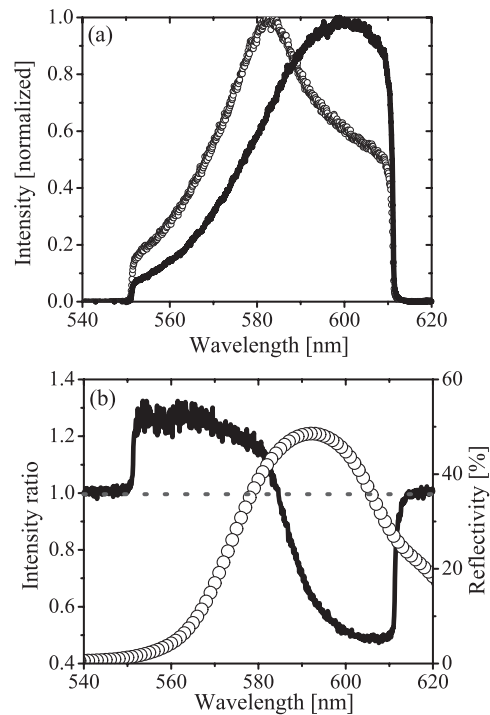

FIG. 3. (a) Emission spectra measured from the photonic crystals composed of dyed-PS spheres of diameter 295 nm (open symbols) and 617 nm (solid line). Emission spectra for photonic crystals of sphere diameter 295 nm show an abrupt decrease in emission intensity around 595 nm due to the photonic stop gap. The emission spectra for photonic crystals of sphere diameter 617 nm do not show any changes in intensity as there is no photonic stop gap in the spectral range of dye emission. (b) The intensity ratio between the emission spectra of photonic crystals with sphere diameter of 295 and 617 nm (solid line) together with corresponding stop gap (open circles) shows the suppression of spontaneous emission in the stop-gap wavelength ranges. The trough in intensity ratio is in good agreement with peak in reflectivity spectra. The intensity ratio is above unity on the blue side of the photonic stop gap.

is not related to the photonic structure. This was confirmed by synthesizing the same structures using nondoped polymer nanospheres. The inset shows the reflectivity peaks between 200 to 400 nm. These are the second- and third-order stop gaps with a low value of reflectance: $\sim 12\%$. In the wavelength range of higher-order stop gaps, the group velocity is reduced due to the flat bands and is an interesting spectral region to be explored. The observation of higher-order stop gaps is another indication of the superior optical quality of the samples [36].

Angle-resolved reflectivity measurements indicate that the stop gaps span over a wavelength range of 602 to 578 nm for an angular range of 15° to 30°. The rhodamine-B dye exhibits emission in the same wavelength range and therefore we expect strong modification of the emission in this angular range. The emission spectra at low excitation energy (0.35 mJ) recorded around 23° to the [111] direction from the dye doped PS photonic crystals of sphere diameter 295 nm (dyed-PS295) and 617 nm (dyed-PS617), is depicted in Fig. 3(a). Here the dyed-PS617 is the reference sample and each emission curve is normalized to its peak value. The pump energy is kept low in order to avoid the participation of any gain effects in the

emission. It is known that the emission features of dyes are sensitive to the solvents, and hence the emission from a liquid solution can differ from the dye-doped polymer. Therefore, a reference sample using the same dye doped into the same polymer needs to be utilized to facilitate a proper comparison. The photonic stop gap of dyed-PS617 is at a wavelength of 1350 nm, and hence the dye emission is insensitive to the photonic stop gap. The higher-order stop gaps for dyed-PS617 appear at 748 nm, 670 nm, and 479 nm, respectively. These higher-order stop gaps also do not overlap with dye emission wavelength range and hence the effect of these stop gaps on the dye emission, in the investigated spectral range, can be neglected in the present work. The emission observed from this sample is, therefore, taken as the intrinsic dye emission. The emission spectrum (solid line) measured from the dyed-PS617 is centered on 600 nm as shown in Fig. 3(a). The emission intensity abruptly goes to zero at the red sides of the emission spectrum due to the limited spectral band of the measurement set up. The emission spectrum from dyed-PS295 is shown by the open symbols in Fig. 3(a), and shows two features. One is the suppression of the emission intensity in a wavelength range of 590 to 605 nm and second, the emission maximum is blueshifted.

Figure 3(b) shows the measured intensity ratio (solid line) between the dyed-PS295 and dyed-PS617 at an angle of incidence of 23°, where the suppression in emission intensity is more evident. The photonic stop gap (open circles) along the [111] direction at the same angle of incidence is also shown in Fig. 3(b). The intensity ratio is expected to be unity for samples in the absence of any stop-gap effect. But in Fig. 3(b), the intensity ratio shows a clear suppression in the wavelength range of 595 to 610 nm, which overlaps with the photonic stop gap along the [111] direction. This is due to the redistribution of the LDOS. The attenuation in emission at the stop gap is quantified by $\Delta I / I_0$ and is estimated to be 51%, which is higher than those reported for dye solution (∼43%) infiltrated in photonic crystals [15]. The peak reflectance value is also ∼50% within the stop gap using external light sources. The stop gap for externally incident light waves (open symbols) and that for internally excited light sources (solid line) are clearly observed in Fig. 3(b). Such a strong modification of emission characteristics in our all-solid photonic crystal is due to the superior quality of the ordering present in our self-assembled photonic crystal structures together with $t > L_B$. We observe in Fig. 3(b) that the intensity ratio is above unity in the blue side of the photonic stop gap. This shows that more photons are emitted on the blue side of the stop gap when the emission is suppressed within the stop gap. The excess emission can be understood as follows: When a source is excited inside the photonic crystal, the emitted light is diffuse and propagates in all possible directions except in the stop gap direction. The diffuse scattered intensity (D), estimated as $D = 1 - (R + T)$, is shown using a blue dotted line in Fig. 2. The diffuse fraction in our samples at the stop gap wavelength is seen to be only 40%, comparable to the best passive samples reported so far [34]. Another point observed in Fig. 2 is the enhancement of diffuse scattered intensity (up to ∼76%) near the blue side of the photonic stop gap. This enhancement manifests itself as a corresponding enhancement in the intensity ratio, seen in Fig. 3(b), at the blue side of the photonic stop gap in the active

photonic crystal. Such an enhancement is understood in terms of an escape function [16,17], which essentially quantifies the escape probability of photons in all directions. This escape function which accounts for the diffuse nature of emitted light shows a large enhancement near the blue side of the stop gap, when the emission is suppressed within the stop gap, as compared to the red side. Therefore, the enhancement in intensity ratio is not observed on the red side of the stop gap.

Next, we analyze the dependence of emission characteristics on the incident pump energy. The emission spectra measured from photonic crystals, as a function of wavelength and for different excitation pump energies, are given for dyed-PS295 and dyed-PS617 in Figs. 4(a) and 4(b), respectively. The corresponding reflectivity spectra are also shown with open symbols. At a low pump energy (0.35 mJ), the spectrum peaks at 583 nm. With further increase in pump energy, it exhibits a redshift and at 7.5 mJ, it peaks at 586 nm. The emission intensity is suppressed in the wavelength region of photonic stop gap irrespective of the pump energy.

At a pump energy of ∼0.7 mJ, we observe the appearance of a sharp peak at ∼606 nm; that is, at the long-wavelength edge of the stop gap [see the vertical dashed line in Fig. 4(a)]. This peak with a narrow width intensifies with pump energy. This peak is absent in the reference sample (dyed-PS617) at any incident pump energy as seen in Fig. 4(b). The peak at 606.41 ± 0.19 nm with a narrow width of 0.78 ± 0.13 nm represents band-edge lasing and occurs at the long-wavelength photonic band edge due to the reduction in the group velocity near the band edges. The LDOS is inversely proportional to group velocity and hence is enhanced near the band edges [37]. The enhancement of LDOS occurs at both the short- and long-wavelength band edge. However, we did not observe any lasing peak near the short-wavelength band edge, irrespective of the incident pump energy, as seen in Fig. 4(a). At the stop-gap wavelength, two standing waves with different frequencies are generated inside the photonic crystal, resulting in the separation of photonic bands, which leads to the opening of a photonic stop gap. The low-frequency modes (long-wavelength band-edge states) concentrate their energy in the high-refractive-index material whereas the high-frequency modes (short-wavelength band-edge states) concentrate their energy in the low-refractive-index material. In our samples, the gain medium is doped into the high-index (polystyrene) material, and hence the low-frequency band-edge states experience gain. The field of the high-frequency band-edge states has a very weak overlap with the gain medium, and hence can be expected to have a very high lasing threshold despite an increase in the LDOS. Therefore, we observe lasing only from the low-frequency (long-wavelength) band-edge states. Thus, we attribute the lasing peak near the long-wavelength photonic band edge to the field-enhancement effect in photonic crystals, in addition to the enhanced LDOS due to low group velocity modes. This confirms that not only the LDOS but also the field distribution at the band-edge frequencies are playing a vital role in band-edge-lasing process.

It can also be noted that, when the lasing threshold is reached near the long-wavelength band edge, the spectrum exhibits a clear trough on the blue side of the lasing peak [marked with diamonds in Fig. 4(a)]. The trough occurs in the immediate vicinity of the lasing peak, and the peak occurs at the edge.
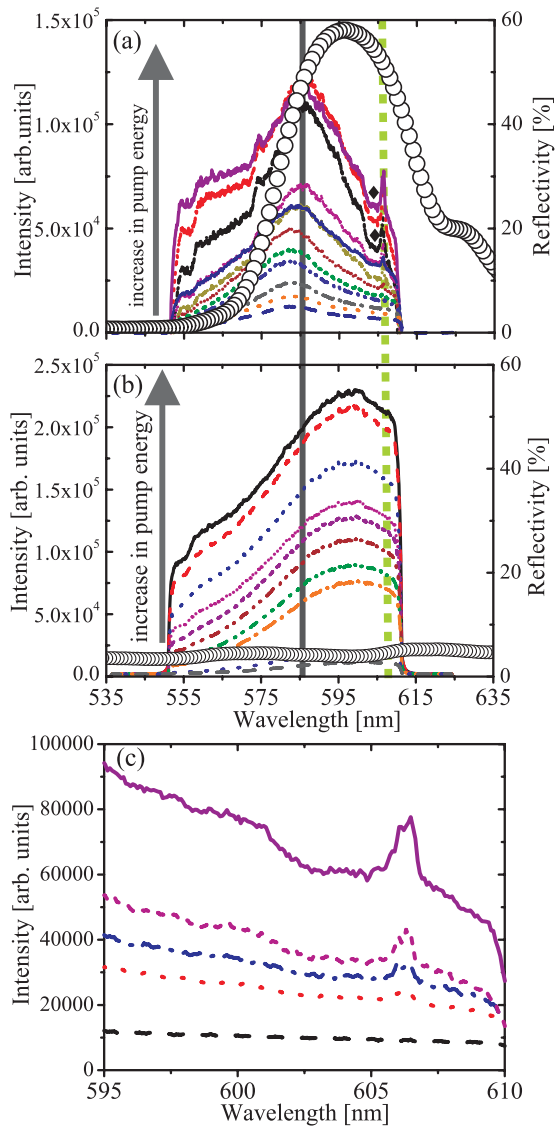
FIG. 4. (Color online) Emission intensity as a function of wavelength with increase in incident pump energy for photonic crystals of sphere diameter (a) 295 nm and (b) 617 nm together with corresponding reflectivity spectra (open symbols). With increasing pump energy, the intensity of emission increases, and a new sharp peak (dashed vertical line) appears near the long-wavelength band edges of the photonic stop gap in (a) which is absent in (b). This represents the band-edge lasing peak. When the lasing peak becomes well resolved, spontaneous emission shows a clear trough (diamond symbol) on the blue of the lasing peak, indicating the removal of energy from spontaneous emission to the stimulated emission. (c) The zoomed-in spectra around the lasing peak at ∼606 nm for different incident pump energies of 0.53 mJ (dashed line), 2.66 mJ (dotted line), 4.09 mJ (dash-dotted line), 7.49 mJ (short dashed line), and 10.98 mJ (solid line). With increasing pump energy, the peak intensifies and slightly shifts to the red side.

We believe the trough originates from the growth of the lasing peak at the cost of spontaneous emission near the edge. This suppression is due to the stimulated emission at the edge frequency which drains the inversion in the active medium, and is over and above the normal stop-gap suppression. It is also seen that, irrespective of the incident pump energy, the emission is
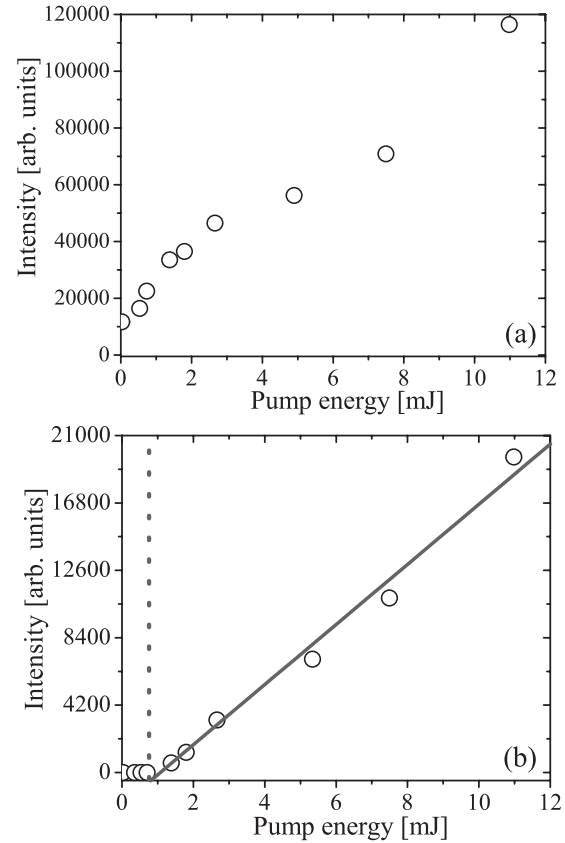

FIG. 5. (a) Amplified spontaneous emission at 586 nm as a function of incident pump energy. A gradual increase in spontaneous emission intensity is evident. (b) The emission intensity of the lasing peak at 606 nm as a function of incident pump energy shows a clear laser threshold at 0.7 mJ (dotted vertical line). Once the threshold is reached, the lasing intensity shoots up.

suppressed in the stop-gap and hence no stop gap lasing is possible. We also observe a gradual narrowing of the broad emission spectra peaking at around 586 nm with increasing pump energy [see vertical solid line in Fig. 4(a)]. This peaking can be attributed to amplified spontaneous emission (ASE) near the blue side of the stop gap and is not due to any kind of lasing. While the 3 nm shift of the ASE peak may point to nonlinear optical effects, we believe the power in our laser is not sufficient to excite such nonlinear effects. Such intensity-dependent photonic-stop-gap shifts in polystyrene photonic crystals have been documented under excitation powers of about 20 GW/cm^2 [38]. Since we work at ∼20 MW/cm^2, we do not expect an appreciable nonlinear excitation in our sample. Rather, such a shift may originate from the emission characteristics of the rhodamine-B dye molecules, wherein the absorption and emission profiles overlap strongly and hence manifest intensity-dependent shifts. Figure 4(c) shows the zoomed-in spectra around the lasing wavelength at different pump energies. Increase in pump energy results in the origin of lasing peak at ∼606 nm. The threshold of band-edge lasing is apparent from the L-L curve for the peaks at ∼606 nm and at ∼586 nm, as shown in Fig. 5. The ASE enhancement at 586 nm is observed as a gradual increase in intensity with increase in incident pump energy as seen in Fig. 5(a). The FWHM for the ASE peak is estimated to be ∼22 nm. A clear threshold

of lasing is observed in the L-L curve at incident energy of 0.7 mJ for the peak at ∼606 nm, as seen in Fig. 5(b). This represents the long-wavelength photonic-band-edge-lasing peak.

IV. CONCLUSIONS

We have demonstrated the signature of photonic-band-edge states on the emission of embedded rhodamine-B dye in a self-assembled all-solid photonic crystal. Our all-solid photonic crystals are easy and quick to fabricate and can provide large area for photonic devices. The samples show well-resolved first- and higher-order photonic stop gaps, which are evidence of their optical quality. Laser-induced-emission experiments show the suppression in emission intensity of ∼51% in the frequency range of the photonic stop gap. With an increase in incident pump energy, we have achieved photonic-band-edge lasing with a lasing threshold of 0.7 mJ. We have explained the origin of lasing as due to the enhancement of LDOS near the band edges and the field-enhancement effect in photonic crystals. The enhancement of emission at certain frequencies can be further exploited for solid state lighting devices. Dye-doped polystyrene is a third-order nonlinear optical material, and hence the refractive index is dependent on the intensity of the incident light. Accordingly, light-induced switching of the stop gap can be implemented, thus achieving optically switchable band-edge lasers. Direction-dependent emission of light in photonic crystals can also be further extended to increase the efficiency of light emitting diodes. The physics of band-edge lasing brought out in the present work is useful in designing nanolasers using CMOS-compatible silicon photonic crystals in the communication wavelength ranges. Another future prospect is to realize three-dimensional cavity structures in which the cavity is all-solid dyed photonic crystal where one expects to have lasing at a much lower threshold value. Thus, our studies open avenues for controlling the light emission using all-solid nanophotonic structures leading to useful applications in optical circuits, communications, sensing, and computing.

[1] C. Santori, D. Fattal, J. Vučkovic, G. S. Solomon, and Y. Yamamoto, Nature (London) **419**, 594 (2002).

[2] O. Painter, R. K. Lee, A. Scherer, A. Yariv, J. D. O'Brien, P. D. Dapkus, and I. Kim, Science **284**, 1819 (1999).

[3] M. Boroditsky, T. F. Krauss, R. Coccioli, R. Vrijen, R. Bhat, and E. Yablonovitch, Appl. Phys. Lett. **75**, 1036 (1999).

[4] L. Zeng, P. Bermel, Y. Yi, B. A. Alamariu, K. A. Broderick, J. Liu, C. Hong, X. Duan, J. D. Joannopoulos, and L. C. Kimerling, Appl. Phys. Lett. **93**, 221105 (2008).

[5] W. L. Vos, A. F. Koenderink, and I. S. Nikolaev, Phys. Rev. A **80**, 053802 (2009).

[6] E. Yablonovitch, Phys. Rev. Lett. **58**, 2059 (1987).

[7] S. John, Phys. Rev. Lett. **58**, 2486 (1987).

[8] S. R. Huisman, R. V. Nair, L. A. Woldering, M. D. Leistikow, A. P. Mosk, and W. L. Vos, Phys. Rev. B **83**, 205313 (2011).

[9] P. Lodahl, A. Floris van Driel, I. S. Nikolaev, A. Irman, K. Overgaag, D. Vanmaekelbergh, and W. L. Vos, Nature (London) **430**, 654 (2004).

[10] S. John and R. Wang, Photonics and Nanostructures-Fundamentals and Applications **2**, 137 (2004).

[11] K. M. Ho, C. T. Chan, and C. M. Soukoulis, Phys. Rev. Lett. **65**, 3152 (1990).

[12] C. Lopez, Adv. Mat. **15**, 1679 (2003).

[13] J. F. Galisteo-López, M. Ibisate, R. Sapienza, L. S. Froufe-Pérez, Á. Blanco, and C. López, Adv. Mat. **23**, 30 (2011).

[14] R. V. Nair, R. Vijaya, K. Kuroda, and K. Sakoda, J. Appl. Phys. **102**, 123106 (2007).

[15] L. Bechger, P. Lodahl, and W. L. Vos, J. Phys. Chem. C **109**, 9980 (2005).

[16] I. S. Nikolaev, P. Lodahl, and W. L. Vos, Phys. Rev. A **71**, 053813 (2005).

[17] A. F. Koenderink and W. L. Vos, Phys. Rev. Lett. **91**, 213902 (2003).

[18] D. Kleppner, Phys. Rev. Lett. **47**, 233 (1981).

[19] Y. Yamamoto, S. Machida, and G. Bjork, Phys. Rev. A **44**, 657 (1991).

[20] X. Hachair, R. Braive, G. L. Lippi, D. Elvira, L. Le Gratiet, A. Lemaitre, I. Abram, I. Sagnes, I. Robert-Philip, and A. Beveratos, Phys. Rev. A **83**, 053836 (2011).

[21] S. John and T. Quang, Phys. Rev. A **50**, 1764 (1994).

[22] L. Florescu, K. Busch, and S. John, J. Opt. Soc. Am. B **19**, 2215 (2002).

[23] P. P. Markowicz, H. Tiryaki, H. Pudavar, P. N. Prasad, N. N. Lepeshkin, and R. W. Boyd, Phys. Rev. Lett. **92**, 083903 (2004).

[24] L. K. Teh, C. C. Wong, H. Y. Yang, S. P. Lau, and S. F. Yu, Appl. Phys. Lett. **91**, 161116 (2007).

[25] M. Scharrer, H. Noh, X. Wu, M. A. Anderson, A. Yamilov, H. Cao, and R. P. H. Chang, J. Opt. **12**, 024007 (2010).

[26] M. Scharrer, A. Yamilov, X. Wu, H. Cao, and R. P. H. Chang, Appl. Phys. Lett. **88**, 201103 (2006).

[27] V. I. Kopp, B. Fan, H. K. M. Vithana, and A. Z. Genack, Opt. Lett. **23**, 1707 (1998).

[28] K. Yoshino, S. Tatsuhara, Y. Kawagishi, M. Ozaki, A. A. Zakhidov, and Z. V. Vardeny, Appl. Phys. Lett. **74**, 2590 (1999).

[29] H. Yamada, T. Nakamura, Y. Yamada, and K. Yano, Adv. Mat. **21**, 4134 (2009).

[30] M. N. Shkunov, Z. V. Vardeny, M. C. DeLong, R. C. Polson, A. A. Zakhidov, and R. H. Baughman, Adv. Fun. Mat. **12**, 21 (2002).

[31] Y. Nishijima, K. Ueno, S. Juodkazis, V. Mizeikis, H. Misawa, M. Maeda, and M. Minaki, Opt. Express **16**, 13676 (2008).

[32] R. V. Nair and R. Vijaya, Appl. Phys. A **90**, 559 (2008).

[33] R. V. Nair and B. N. Jagatap, Phys. Rev. A **85**, 013829 (2012).

[34] S. G. Romanov, M. Bardosova, D. E. Whitehead, I. M. Povey, M. Pemble, and C. M. Sotomayor Torres, Appl. Phys. Lett. **90**, 133101 (2007).

[35] J. F. Galisteo-López, E. Palacios-Lidón, E. Castillo-Martínez, and C. López, Phys. Rev. B **68**, 115109 (2003).

[36] R. V. Nair and R. Vijaya, Phys. Rev. A **76**, 053805 (2007).

[37] J. M. Bendickson, J. P. Dowling, and M. Scalora, Phys. Rev. E **53**, 4107 (1996).

[38] Y. Liu, F. Qin, Z.-Y. Wei, Q.-B. Meng, D.-Z. Zhang, and Z.-Y. Li, Appl. Phys. Lett. **95**, 131116 (2009).